

# Surface-Plasmon-Mediated Gradient Force Enhancement and Mechanical State Transitions of Graphene Sheets

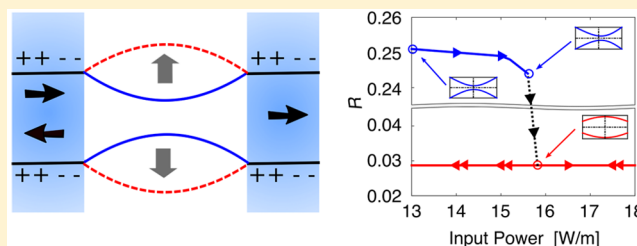
Peng Zhang,<sup>†</sup> Nian-Hai Shen,<sup>\*,†,‡</sup> Thomas Koschny,<sup>†</sup> and Costas M. Soukoulis<sup>\*,†,‡</sup>

<sup>†</sup>Ames Laboratory and Department of Physics and Astronomy, Iowa State University, Ames, Iowa 50011, United States

<sup>‡</sup>Institute of Electronic Structure and Laser, FORTH, 71110 Heraklion, Crete, Greece

**ABSTRACT:** Graphene, a two-dimensional material possessing extraordinary properties in electronics as well as mechanics, provides a great platform for various optoelectronic and optomechanical devices. Here, we theoretically study the optical gradient force arising from the coupling of surface plasmon modes on parallel graphene sheets, which can be several orders stronger than that between regular dielectric waveguides. Furthermore, with an energy functional optimization model, possible force-induced deformation of graphene sheets is calculated. We show that the significantly enhanced optical gradient force may lead to mechanical state transitions of graphene sheets, which are accompanied by abrupt changes in reflection and transmission spectra of the system. Our demonstrations illustrate the potential for broader graphene-related applications such as force sensors and actuators.

**KEYWORDS:** graphene, optical gradient force, surface plasmon, mechanical state transition



Light–matter interactions exist in various forms, and optical force is one of the most intuitive representations. A well-known phenomenon showing the effect of optical force is the deflection of the comet tail pointing away from the sun due to the solar radiational pressure. Recently, people have been exploring the possibilities of utilizing optical force in micro- and nanosystems for a variety of practical applications, such as optical tweezers<sup>1</sup> and controlling photonic circuits.<sup>2</sup> However, under many circumstances, the optomechanical effects are fairly inconspicuous due to weak light–matter interactions. Therefore, many efforts have been taken toward the enhancement of optical forces.<sup>3–5</sup>

Graphene, a two-dimensional (2D) material composed of one layer of carbon atoms in a honeycomb lattice, has attracted intensive attention due to its unique properties in various aspects.<sup>6,7</sup> In particular, graphene provides a new platform for a variety of intriguing optoelectronic and optomechanical effects. The highly reactive electric response of graphene results in strongly localized plasmons residing within the deep sub-wavelength region, which leads to a prosperous subfield named graphene plasmonics with plenty of promising applications ranging from the terahertz (THz) to the infrared regime.<sup>8–11</sup> Graphene also has been shown to possess superior mechanical properties, such as strong in-plane stiffness with a measured Young's modulus as high as 1 TPa,<sup>12</sup> several orders larger than that of conventional materials. Considering its extremely small mass density as a 2D material, graphene therefore provides a great opportunity in force sensing and many other practical applications.<sup>13–16</sup>

In this paper, we investigate the interaction (optical gradient force) between two graphene sheets, which may be adopted in micro- and nanomechanical systems, and reveal that such force

originating from the coupled surface-plasmon-polariton (SPP) modes of graphene layers can be greatly enhanced to several orders stronger than that of a regular parallel-waveguide system (Section II). In addition, in a cavity-like system with precurved graphene sheets, we explore the potential configurations of deformation—mechanical states—under certain bending energy. Arising from the strongly enhanced gradient force between graphene layers, the phenomena of mechanical state transitions are demonstrated, accompanied by abrupt changes in reflection and transmission spectra of the system (Section III). Our work will be beneficial for various designs of graphene-based optomechanical devices, such as force sensors, actuators, and optical switches.

## ■ STRONGLY ENHANCED GRADIENT FORCE BETWEEN GRAPHENE LAYERS

In general, the dipole approximation classifies optical forces into two main categories, i.e., radiational force and gradient force.<sup>17</sup> The radiational force is directly associated with the wave-vector of light and is interpreted as the momentum interchange between light and matter when the propagation path is altered due to the inhomogeneity of the space.<sup>18,19</sup> The optical gradient force essentially refers to the gradient of field energy, which plays an important role in integrated optics and has been intensively studied in coupled waveguide systems.<sup>2,3,20–27</sup> For two dielectric slab waveguides (thickness  $t$ ), settled in parallel with separation  $d_w$  as shown in Figure 1b, the tails of fields for waveguide modes interact with each other, introducing a force perpendicular to the propagation direction.

Received: November 4, 2016

Published: December 16, 2016

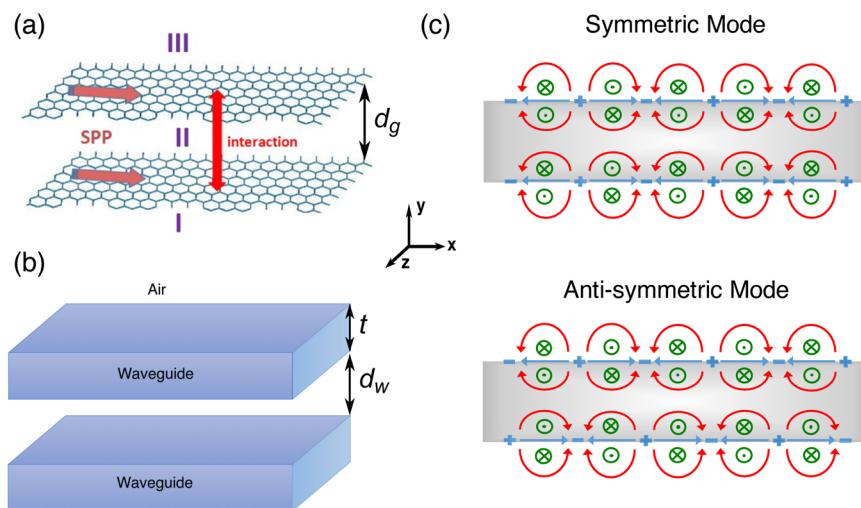


**Figure 1.** Schematic configurations of parallel graphene sheets (a) and parallel dielectric waveguides (b). Surface plasmons, propagating along the  $x$ -direction of either a symmetric or antisymmetric mode (c), induce interactions between graphene sheets. Signs “+” and “-” denote the oscillating surface charges. Straight and curved arrows show the directions of surface currents and electric fields, respectively. Circled cross and dot symbols indicate the magnetic fields.

Mimicking the case of a parallel-waveguide system, here, we consider the interaction between two graphene layers upon the excitation of SPP modes, the field of which decays away from graphene at both sides (see Figure 1a). It is noted that the coupled SPP modes can be classified as symmetric or antisymmetric, depending on the relative phase of surface currents or electromagnetic (EM) fields (see Figure 1c). For uniform notation, we denote the symmetry of the coupled SPP modes based on the symmetry of surface currents throughout the paper, since the currents and fields may show opposite symmetry.

Figure 2a shows the comparison of the dispersion relations for SPP modes of two coupled graphene sheets ( $d_g = 100$  nm) and  $TM_0$  modes (magnetic field  $H$  along the  $z$ -direction) of two coupled slab waveguides ( $d_w = 100$  nm) made from silicon with refractive index  $n = 3.48$ .<sup>3</sup> For the parallel-waveguide configuration, two different thicknesses are considered, i.e.,  $t = 1.5$  and  $2.5$   $\mu\text{m}$ , respectively. From Figure 2a, we can clearly see the advantages of coupled graphene sheets mainly in two aspects: much better separated modes in dispersion relation imply a much stronger coupling effect between graphene layers, and the settlement of modes much further away from the light line (dash-dotted line in Figure 2a) illustrates a stronger localization of SPPs, leading to a much larger field gradient in the ambient medium (air) and therefore the force as well. By setting the frequency to 40.4 THz, we show in Figure 2b the eigenvalues of the propagation constant of coupled SPP modes ( $k_{\text{SPP}}$ ) dependent on the separation constant between graphene sheets,  $d_g$ . When the two graphene layers are well separated, i.e.,  $d_g$  is large enough, the coupling in-between can be neglected and, correspondingly, the symmetric (solid line) and antisymmetric (dashed line) modes are degenerate. As the separation  $d_g$  decreases, the interaction between graphene layers gets stronger and the degeneracy of SPP modes breaks eventually.

To provide an intuitive analysis to the gradient force in the aforementioned parallel-graphene-layer or parallel-waveguide system, we can consider both of the graphene layers or waveguides as two adjacent finite-potential wells. Although light is confined on the graphene sheets or inside the waveguides, the quantum tunneling effect still allows the photons to

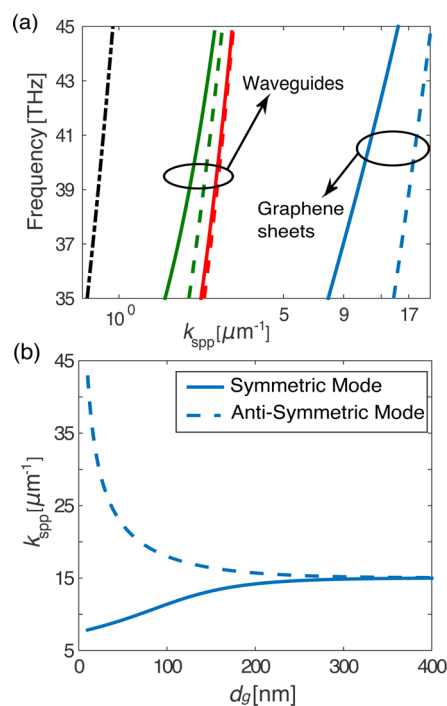


**Figure 2.** (a) Dispersion relations for SPP modes of parallel graphene sheets in comparison to  $TM$  modes of the parallel dielectric waveguides ( $\epsilon_d = 3.8$ ) with  $t = 1.5$  (left set in green) and  $2.5$   $\mu\text{m}$  (right set in red).  $d_g = d_w = 100$  nm. The case of the light line (dash-dotted line) is set as a reference. Solid (dashed) lines correspond to the symmetric (antisymmetric) modes. The green (red) lines correspond to the modes in a pair of dielectric slabs with a thickness of 1.5  $\mu\text{m}$  (2.5  $\mu\text{m}$ ). (b)  $k_{\text{SPP}}-d_g$  dependency for parallel graphene sheets at 40.4 THz: symmetric (solid line) and antisymmetric (dashed line) modes.

transmit from one to the other, and it is this exchange of photons that leads to the gradient force. Assuming  $U = N\hbar\omega$ , representing the coupled EM field energy, where  $N$  is the number of photons,  $\hbar$  the reduced Planck constant, and  $\omega$  the circular frequency of the EM wave, the induced gradient force can be expressed as follows:<sup>26</sup>

$$F = -\frac{\partial U}{\partial y} = -\frac{U}{\omega} \frac{\partial \omega}{\partial y} \Big|_{k_{\text{spp}}} \quad (1)$$

It must be noted that  $\omega$ ,  $y$ , and  $k_{\text{spp}}$  are not independent, but tied with each other under the following dispersion relation of the coupled graphene SPPs:

$$\kappa(\pm e^{-\kappa d_g} - 1) = -i \frac{2\omega\epsilon_0}{\sigma_s} \quad (2)$$

where  $\kappa = (k_{\text{spp}}^2 - k_0^2)^{1/2}$  denotes the decaying factor and  $\sigma_s$  is the surface conductivity of graphene. In the long-wavelength and high doping limits under our consideration, the optical conductivity  $\sigma_s$  is dominated by the intraband transitions, which follow the local Drude model expressed as<sup>28</sup>

$$\sigma_s(\omega) = \frac{e^2 E_F}{\pi \hbar^2 (\tau^{-1} - i\omega)} = \frac{\alpha}{\gamma - i\omega} \quad (3)$$

where  $e$  is electronic charge,  $E_F$  is the doped Fermi level,  $\gamma = \tau^{-1}$  is the collision frequency with  $\tau$  denoting the momentum relaxation time, and  $\alpha$  is the so-called Drude weight. In our following calculations, we assume  $\alpha = 7.6 \times 10^{10} (\Omega\text{s})^{-1}$  and  $\gamma = 1.89 \text{ THz}$ , as reported in ref 29.

From the implicit function theorem for differentiation of dependent variables,<sup>30</sup> the gradient force  $F$  in eq 1 can be rewritten in the form of

$$F = + \frac{U}{\omega} \frac{\partial \omega}{\partial k_{\text{spp}}} \Big|_y \frac{\partial k_{\text{spp}}}{\partial y} \Big|_{\omega} \quad (4)$$

and, qualitatively, we can determine whether the force  $F$  is attractive (negative sign) or repulsive (positive sign) based on Figure 2; that is, the antisymmetric (symmetric) mode corresponds to an attractive (repulsive) force. We can also understand the nature of such a force in an intuitive view considering the oscillating charges. Taking the symmetric-mode case as an example where both currents and charges are in phase, the in-phase currents result in an attractive force, while the charges with the same sign will lead to a repulsive force. Therefore, a competition exists between the forces arising from the currents and charges, which determines the net force, and in our configuration of parallel graphene layers, we can find the interaction of charges plays a dominant role.

Quantitatively, we can calculate the time-averaged force between graphene layers with Maxwell's stress tensor  $\vec{T}$ :<sup>17</sup>

$$\langle F_i \rangle = \oint_S \langle T_{ij} \rangle n_j \, dS \quad (5)$$

where the tensor element  $T_{ij}$  is in the form of EM fields as

$$T_{ij} = \epsilon_0 \left( E_i E_j - \frac{1}{2} \delta_{ij} E^2 \right) + \mu_0 \left( H_i H_j - \frac{1}{2} \delta_{ij} H^2 \right) \quad (6)$$

Figure 3 shows the comparison of calculated forces (plotted with absolute values in log scale) for the configurations of parallel graphene layers and parallel waveguides, where the separations in-between are set the same with  $d_g = d_w = 100 \text{ nm}$ . Two different thicknesses, i.e.,  $t = 1.5$  and  $2.5 \mu\text{m}$ , are considered for the parallel-waveguide case, and as expected, thinner slabs show a stronger force since the thicker the slabs, the stronger the confinement of EM fields inside the waveguides but the weaker the fields outside, leading to a weaker interaction in between. From Figure 3, we are amazed to see that the force between graphene layers can be several orders

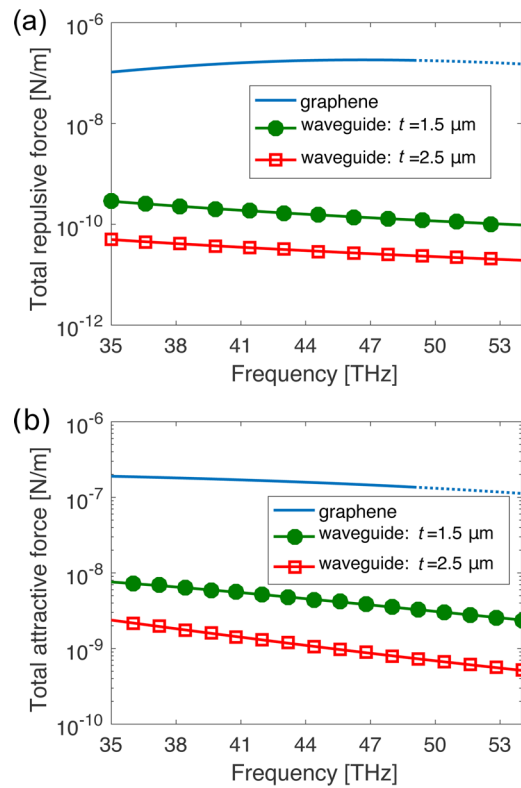


**Figure 3.** Comparisons of optical force for parallel-graphene-sheet and parallel-waveguide configurations with the same separation 100 nm in-between: (a) repulsive force for symmetric mode; (b) attractive force for antisymmetric mode. The input power is set as 1 W/m.

stronger than that in the waveguide cases, and such a dramatic enhancement of interaction, originating from much larger field gradients in the ambient medium (see dispersion relations in Figure 2 for direct evidence), will be greatly beneficial for various practical applications in optomechanical systems. We also notice from Figure 3 that the gradient optical force between graphene layers does not change monotonically with frequency. This can be understood qualitatively via the expression of the force  $F \propto (\kappa^2/\omega^2)e^{-\kappa d_g}$ , calculated from the Maxwell stress tensor. Therefore, the force is determined by two competitive aspects, i.e.,  $\kappa$ , which represents the gradient of the field, and  $e^{-\kappa d_g}$ , which corresponds to the field strength at the evanescent tail. At the low frequency side, the system has a smaller  $k_{\text{spp}}$  and correspondingly smaller  $\kappa$  (see Figure 2a), which means the EM field between layers is stronger but with a lower gradient. Therefore, the strength of the field dominates over the gradient for the force at low frequencies. It is the opposite case for high frequencies, where the gradient of the field is large, while with a weak field strength. A trade-off does exist leading to the strongest force. It is noted that the force of parallel graphene layers at frequencies over 50 THz are marked with a dotted line in Figure 3, since the actual force would be smaller due to extra losses induced by phonon–electron interactions.

## MECHANICAL STATE TRANSITIONS

In Section II, we have demonstrated an SPP-induced significant force enhancement between parallel graphene layers in the infrared regime, i.e., several orders stronger than that between parallel waveguides. Therefore, the introduction of graphene in micro- or nanosystems is believed to result in various

interesting optomechanical effects. As well-known, from classical mechanics, a thin plate can be bent if a force or torque is exerted. In this section, we will construct a conceptual configuration with two graphene layers settled closely to each other and explore the deflections of graphene sheets, even the possibilities of mechanical state variations, which will provide solid physical foundations and guidances toward various practical applications in optomechanics.

Generally, considering the bending of a classical thin shell, the middle plane keeps its original length, while the planes above and below are stretched and compressed, respectively, resulting in a bending energy in comparison to its free state. Under small deflections, the level of bending can be described using a linear model and is related to a material-dependent constant, the so-called bending stiffness,  $D \propto Eh^3$ ,<sup>31</sup> where  $E$  is the bulk Young's modulus and  $h$  is the thickness of the thin plate. In contrast, graphene, as a 2D material, has no well-defined thickness. Therefore, a different origin of rigidity corresponds to free bending of graphene sheets; that is, instead of any stretch or compression, the bending energy of graphene arises from the rotation of C–C bonds since the  $sp^2$  hybridization tends to keep the carbon atoms in plane, and accordingly, the Kirchhoff theory for classical thin plates no longer holds.<sup>32</sup> Theoretically, the bending modulus  $D$  can be obtained from ab initio calculations, and the most commonly used value is 0.192 nN·nm.<sup>13,33–37</sup> In our work, we will adopt a phenomenological model to investigate the bending of graphene sheets. Under small deformations, the linear model applies:  $F = F_b + F_s$ , with  $F_s$  being the in-plane stretch energy and  $F_b$  the pure bending energy,  $F_b = \int \frac{1}{2} D \kappa^2 ds$ ,<sup>32</sup> respectively, where  $\kappa = y'' / (1 + y'^2)^{3/2}$  denotes the curvature of the bent graphene sheet.

Figure 4 shows the schematic of our setup, in which two graphene layers with the separation  $d_g = 100$  nm are embedded in some dielectric medium ( $\epsilon_d$  is taken as 3.8) at two sides. The

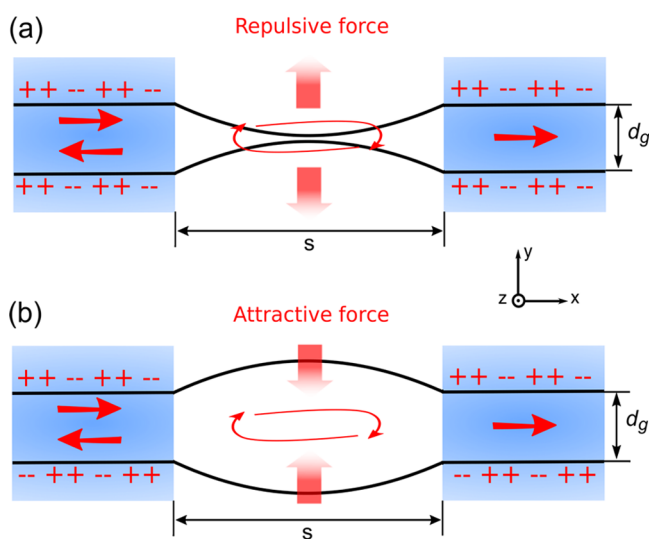


**Figure 4.** Schematic configuration of the constructed system for demonstrating optical-force-induced mechanical state transitions of graphene sheets: (a) initial state of the concave configuration with symmetric mode injection; (b) initial state of the convex configuration with antisymmetric mode injection. Graphene layers are embedded in a dielectric medium at two sides ( $s = 1 \mu\text{m}$ ) with precurved shape in between (length  $1.004 \mu\text{m}$ ).

distance between two-sided dielectric blocks,  $s$ , is  $1 \mu\text{m}$ , while the length of the graphene sheets in-between is assumed to be  $1.004 \mu\text{m}$ , so that the graphene layers are in a curved status for demonstrating optomechanical deflections, and different shapes of graphene sheets correspond to different mechanical energy states. Intuitively, the lowest state, denoted as the ground state, should have a cosine-like shape with only one antinode, the first metastable state will correspond to a sine-like shape with two antinodes, and higher order states possess a certain number of antinodes. Assuming the parallel graphene sheets sit at the ground state initially, they may be in either concave (Figure 4a) or convex (Figure 4b) configurations, which are degenerate without an external force. In the case of some force being applied to the system, such a degeneracy will be broken and one configuration experiences lower energy than the other. Therefore, an optical-gradient-force-induced mechanical state transition may be achieved.

In Figure 4a, the two graphene sheets are initially in the concave configuration, to which we inject the symmetric SPP mode with a certain power from one side, leading to a repulsive force between the graphene sheets. Upon increasing the input power, the force gets stronger accordingly, and at some threshold point, the graphene sheets get flipped and reach the state of a convex configuration. It should be noted that, as long as the graphene sheets flip over, the effective gap in-between changes and the eigenvalue of the propagation constant of the coupled SPPs also changes accordingly. In the EM view, the two-sided dielectric blocks naturally form a Fabry–Pérot (FP) cavity in-between for SPP waves of graphene, and the transmission ( $T$ ) and reflection ( $R$ ) of the system may vary dramatically upon the shape change of the graphene sheets, providing an excellent and straightforward strategy of monitoring the mechanical state transition macroscopically.

We apply a self-consistent iterative method to find the corresponding deformations of the graphene sheets. Considering the optical force is fairly small compared to the strong in-plane modulus of graphene, we assume no in-plane stretch or compression happens in our discussions, implying a constraint of the length of graphene sheets in the cavity being kept as  $1.004 \mu\text{m}$ . Therefore, the problem of finding the shape configurations for graphene sheets turns out to be optimizing the energy function for a local minimum under the length constraint. Under external fields, the bending energy density function can be written as follows in the form of deformation:

$$F[w(x)] = \int \frac{1}{2} D \kappa^2 ds - \int f_{\text{optical}} [w(x)] \Delta w(x) dx \quad (7)$$

where the energy density  $F$ , in units of J/m, represents the total energy per unit length in the  $z$ -direction of graphene,  $w(x)$  is the function of deformation with respect to the coordination along the  $x$ -direction,  $\kappa = w''(x) [1 + w'(x)^2]^{-3/2}$  is the local curvature, and  $ds = [1 + w'(x)^2]^{-1/2} dx$  is the arc length. Technically, to figure out the local minimum of the energy function, we utilize the so-called “steepest decent” method<sup>38</sup> by performing Fourier expansions to the deformation function  $w(x)$  and applying the optical force of the initial configuration. As long as a new configuration of deformation is reached, the corresponding optical gradient force of the graphene system is calculated and substituted into the energy function for another round of optimization. Iterations continue until the deformation configuration does not change, reaching a converged and final state.

As stated in the above, we can monitor the mechanical deformation of graphene sheets via the propagation properties of EM waves ( $R$  and  $T$ ) in the system. For a better contrast in  $R$  and  $T$  spectra between the concave and convex configurations (see Figure 5), we can choose some demonstration frequency

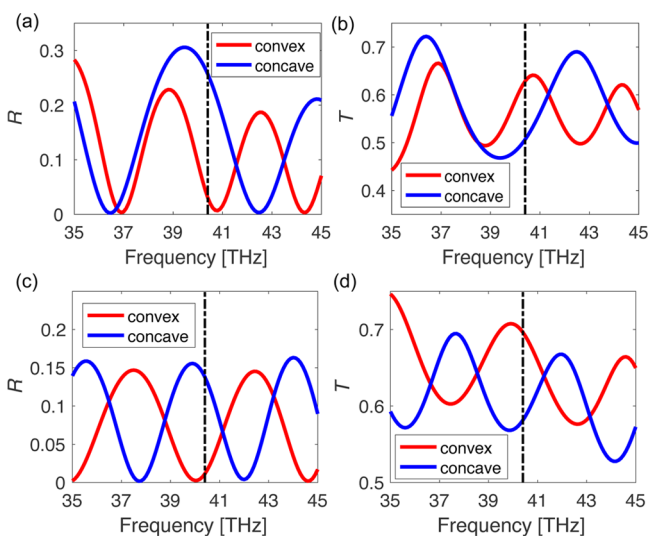


**Figure 5.** Calculated reflection ( $R$ ) and transmission ( $T$ ) spectra for concave (blue dark line) and convex (red light line) configurations of graphene sheets under symmetric (a and b) and antisymmetric (c and d) SPP modes. Dash dotted lines correspond to the frequency 40.4 THz, where significant contrast in  $R$  and  $T$  exists between the concave and convex configurations.

accordingly, and in our following discussions, we set it as 40.4 THz, at which the concave (convex) configuration has  $R = 25.1\%$  (2.9%) and  $T = 51.0\%$  (63.0%) under symmetric SPP modes, while  $R = 13.8\%$  (1.3%) and  $T = 58.0\%$  (69.4%) for antisymmetric SPP modes, respectively.

Figure 6 shows the processes of mechanical state transitions with respect to input powers, calculated via the previously

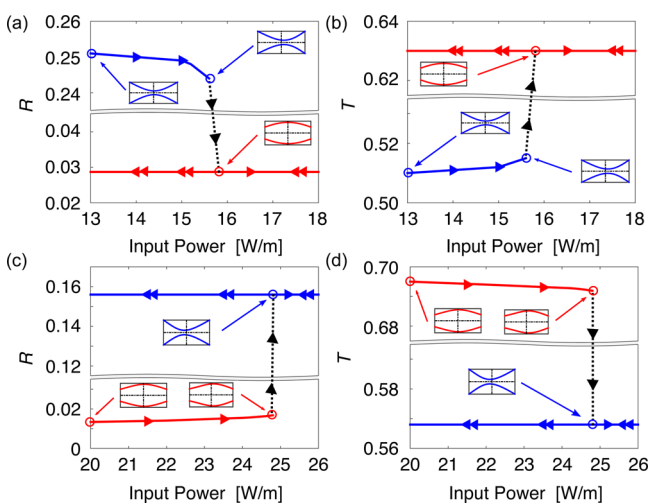


**Figure 6.** Monitored  $R$  and  $T$  dependent on the input power showing the processes of mechanical state transitions: symmetric mode (a and b) and antisymmetric mode (c and d). Single arrows mark the direction of the transition path from initial state toward final state upon the increase of input power, while double arrows indicate that the final state does not vary when the input power decreases.

described iterative method. Figure 6a and b correspond to the case with symmetric SPP mode injection in the graphene sheets. For the initial state being the concave configuration, the increase of the input power (the path is marked with single arrows) leads to slight deformations initially, but abrupt changes in  $R$  and  $T$  spectra happen at the input power of 15.8 W/m, the threshold for the mechanical state transition, where the graphene sheets flip to the convex configuration. Upon the decrease of input power for the convex configuration, the repulsive force induced by symmetric SPP modes keeps the graphene configuration, and there is no change in  $R$  or  $T$  (see Figure 6a and b), consistent with our intuitive expectations. Figure 6c and d show the case of antisymmetric SPP mode injection with attractive gradient force between graphene sheets: Starting from the convex configuration, the increase of input power (direction along single arrows) induces some slight deformations to the graphene sheets initially, and the mechanical state transition occurs at 25.0 W/m, with evidence of abrupt changes in  $R$  and  $T$  spectra. It should be noted that  $R$  and  $T$  of the final state in Figure 6c and d are to some extent different from those values calculated for the concave ground state, which means such a final state is not exactly the ground state and may be called a pseudo-concave configuration. This will be further explained by working out the transition path and the corresponding force density profiles shown in Figure 7. The same as the case of symmetric SPP modes, upon the decrease of input power from the pseudoconcave configuration, the shape of graphene sheets does not change with constant  $R$  and  $T$ , marked with double arrows in Figure 6c and d. In addition, it should be noted that in Figure 6, if the injected power keeps increasing beyond the mechanical state transition, the gradient force will eventually get extremely strong, leading to the in-plane deformation of the graphene sheets and corresponding change of monitored propagation properties ( $R$  and  $T$ ) of the system. For accurate calculations under high enough input power, our initial model, which is based on the fixed-length constraint neglecting any in-plane deformation, needs to be modified accordingly by introducing a real in-plane elastic modulus to optimize the total energy function.

We reveal under symmetric SPP mode how the mechanical state of the graphene sheets transits from the concave configuration to the convex one upon the threshold input power (transition window marked with dotted lines in Figure 6a and b), by showing the geometric-deformation and force-density profiles in Figure 7a and b, respectively. The induced gradient force is stronger at the injection side (left), so the shape of graphene sheets starts changing from the left and reaches the final state by experiencing two-antinode profiles. It is noted that the three middle profiles (marked with a dotted lines) do not correspond to any metastable state, but are obtained in our iterative procedure only for illustrating the instant transition path near the threshold point. The mechanical transition for the antisymmetric SPP mode behaves similarly, whose geometric-deformation and force-density profiles neighboring the threshold are presented in Figure 7c and d; that is, the graphene sheets have their left parts dragged first due to a stronger repulsive force induced at the injection side and transit to a final concave state, experiencing some two-antinode profiles as well. However, due to the strong but asymmetric repulsive force, the final concave state is not symmetric but slightly biased to the left, showing  $R$  and  $T$  different from those are in the symmetric concave “ground state”. In addition, we need to point out that, along the

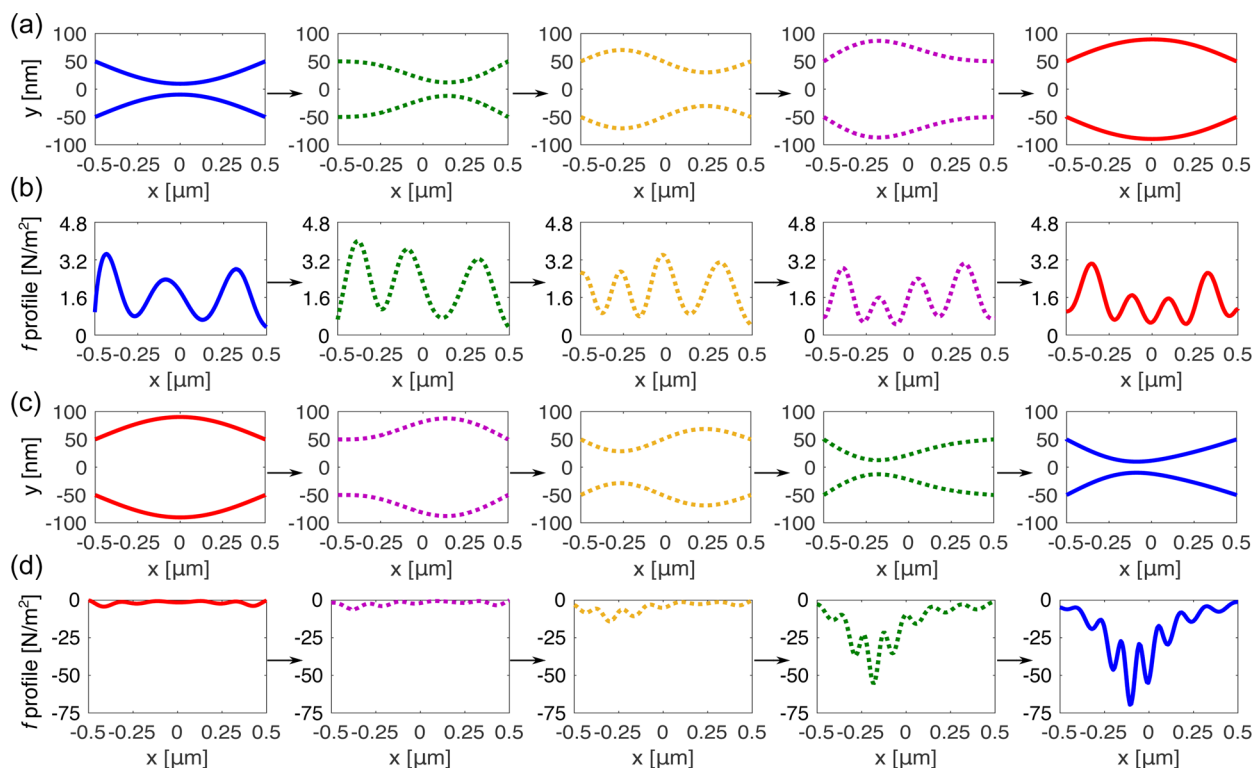


**Figure 7.** Variation of geometric-configuration and force-density profiles for graphene sheets from initial state to final state under symmetric mode (a and b) and antisymmetric mode (c and d), respectively. The three intermediate cases (dotted lines) are not metastable states but only indicate the process of the mechanical state transition being reached. The input power is taken with the threshold value, i.e., 15.8 W/m and 25 W/m for symmetric and antisymmetric mode, respectively.

transition path (marked with single arrows in Figure 6), any point on the solid lines corresponds to a metastable state; that is, before we reach the transition point, switching off the input power leads the graphene sheets back to the initial state, and beyond the threshold, the release of the force will retain the configuration of the graphene sheets in the new state.

It may also be noted from Figure 7b and d that, during the demonstrated mechanical state transitions, the antisymmetric mode experiences a significant change in the corresponding attractive force, but the repulsive force remains more or less the same under the symmetric mode. Equation 4 indeed shows that the gradient optical force between graphene sheets is proportional to the first derivative of  $k_{\text{spp}}$  to  $d_g$ . For the antisymmetric mode, the transition from convex configuration to concave state leads to the abrupt decrease of effective separation between graphene sheets, and as indicated with a dashed line in Figure 2b, there exists a sharp dependence of  $k_{\text{spp}}$  with respect to  $d_g$  at the side of a small separation in-between and very strong attractive force correspondingly. In contrast, the symmetric mode has a fairly gentle dependence between  $k_{\text{spp}}$  and  $d_g$  (see solid line in Figure 2b), which indicates there is no dramatic change in the repulsive force under the transition from concave to convex configuration. Moreover, in our meticulous calculations, we noticed the repulsive force under the symmetric mode experiences a tendency of first getting stronger and then weaker during the mechanical state transition, while the antisymmetric mode shows a monotonic change in the attractive force. According to eq 4, the second derivative of  $k_{\text{spp}}$  to  $d_g$  determines the tendency of gradient force, and only the case of the symmetric mode possesses an

inflection point with  $d_g$  around 70 nm (see Figure 2b), where the repulsive force is the strongest.

## CONCLUSION

In conclusion, our work showed a significant enhancement of optical gradient force between graphene sheets induced by coupled surface plasmon polaritons. Such a force can be several orders stronger than that existing between regular dielectric waveguides and definitely will open up new avenues for efficient control of micro- and nanocomponents in optomechanical systems. As one of the fundamental phenomena, we demonstrated optical-force-induced mechanical state transitions for curved neighboring graphene sheets, which were intuitively characterized via electromagnetic spectra measurements in a constructed cavity-like system. Our investigations therefore will be greatly beneficial for the exploration of various new optomechanical devices integrated with graphene, such as force sensors, actuators, and optical switches.

## AUTHOR INFORMATION

### Corresponding Authors

\*E-mail: nhshen@ameslab.gov.

\*E-mail: soukoulis@ameslab.gov.

### ORCID

Nian-Hai Shen: 0000-0002-9715-0130

### Notes

The authors declare no competing financial interest.

## ACKNOWLEDGMENTS

P.Z. and N.-H.S. thank Y. Sun, X. Zhao, and C. Liu for helpful discussions on computational techniques and optimization

methods. Work at Ames Lab was partially supported by the U.S. Department of Energy, Office of Basic Energy Science, Division of Materials Sciences and Engineering (Ames Laboratory is operated for the U.S. Department of Energy by Iowa State University under Contract No. DE-AC02-07CH11358), by the U.S. Office of Naval Research Award No. N00014-14-1-0474 (simulations), and by ERC Grant No. 320081 (PHOTOMETA) (theory).

## REFERENCES

- (1) Novotny, L.; Bian, R. X.; Xie, X. S. Theory of Nanometric Optical Tweezers. *Phys. Rev. Lett.* **1997**, *79*, 645–648.
- (2) Wiederhecker, G. S.; Chen, L.; Gondarenko, A.; Lipson, M. Controlling photonic structures using optical forces. *Nature* **2009**, *462*, 633–636.
- (3) Ginis, V.; Tassin, P.; Soukoulis, C. M.; Veretennicoff, I. Enhancing Optical Gradient Forces with Metamaterials. *Phys. Rev. Lett.* **2013**, *110*, 057401.
- (4) Intaraprasong, V.; Fan, S. Enhancing the waveguide-resonator optical force with an all-optical on-chip analog of electromagnetically induced transparency. *Phys. Rev. A: At., Mol., Opt. Phys.* **2012**, *86*, 063833.
- (5) Huang, C.; Zhu, L. Enhanced optical forces in 2D hybrid and plasmonic waveguides. *Opt. Lett.* **2010**, *35*, 1563–1565.
- (6) Novoselov, K. S.; Geim, A. K.; Morozov, S. V.; Jiang, D.; Zhang, Y.; Dubonos, S. V.; Grigorieva, I. V.; Firsov, A. A. Electric Field Effect in Atomically Thin Carbon Films. *Science* **2004**, *306*, 666–669.
- (7) Geim, A. K.; Novoselov, K. S. The rise of graphene. *Nat. Mater.* **2007**, *6*, 183–191.
- (8) Jablan, M.; Soljacic, M.; Buljan, H. Plasmons in Graphene: Fundamental Properties and Potential Applications. *Proc. IEEE* **2013**, *101*, 1689–1704.
- (9) Low, T.; Avouris, P. Graphene Plasmonics for Terahertz to Mid-Infrared Applications. *ACS Nano* **2014**, *8*, 1086–1101.
- (10) Tassin, P.; Koschny, T.; Soukoulis, C. M. Graphene for Terahertz Applications. *Science* **2013**, *341*, 620–621.
- (11) Tassin, P.; Koschny, T.; Kafesaki, M.; Soukoulis, C. M. A comparison of graphene, superconductors and metals as conductors for metamaterials and plasmonics. *Nat. Photonics* **2012**, *6*, 259–264.
- (12) Lee, C.; Wei, X.; Kysar, J. W.; Hone, J. Measurement of the Elastic Properties and Intrinsic Strength of Monolayer Graphene. *Science* **2008**, *321*, 385–388.
- (13) Croy, A.; Midtvedt, D.; Isacsson, A.; Kinaret, J. M. Nonlinear damping in graphene resonators. *Phys. Rev. B: Condens. Matter Mater. Phys.* **2012**, *86*, 235435.
- (14) Eichenfield, M.; Camacho, R.; Chan, J.; Vahala, K. J.; Painter, O. A picogram- and nanometre-scale photonic-crystal optomechanical cavity. *Nature* **2009**, *459*, 550–555.
- (15) Song, X.; Oksanen, M.; Li, J.; Hakonen, P. J.; Sillanpää, M. A. Graphene Optomechanics Realized at Microwave Frequencies. *Phys. Rev. Lett.* **2014**, *113*, 027404.
- (16) Singh, V.; Bosman, S. J.; Schneider, B. H.; Blanter, Y. M.; Castellanos-Gomez, A.; Steele, G. A. Optomechanical coupling between a multilayer graphene mechanical resonator and a superconducting microwave cavity. *Nat. Nanotechnol.* **2014**, *9*, 820–824.
- (17) Novotny, L. *Principles of Nano-optics*; Cambridge University Press: Cambridge, 2012.
- (18) Chen, J.; Ng, J.; Lin, Z.; Chan, C. T. Optical pulling force. *Nat. Photonics* **2011**, *5*, 531–534.
- (19) Zhang, J.; MacDonald, K. F.; Zheludev, N. I. Optical gecko toe: Optically controlled attractive near-field forces between plasmonic metamaterials and dielectric or metal surfaces. *Phys. Rev. B: Condens. Matter Mater. Phys.* **2012**, *85*, 205123.
- (20) Eichenfield, M.; Michael, C. P.; Perahia, R.; Painter, O. Actuation of micro-optomechanical systems via cavity-enhanced optical dipole forces. *Nat. Photonics* **2007**, *1*, 416–422.
- (21) Ma, J.; Povinelli, M. L. Applications of optomechanical effects for on-chip manipulation of light signals. *Curr. Opin. Solid State Mater. Sci.* **2012**, *16*, 82–90.
- (22) Van Thourhout, D.; Roels, J. Optomechanical device actuation through the optical gradient force. *Nat. Photonics* **2010**, *4*, 211–217.
- (23) Roels, J.; De Vlamincq, I.; Lagae, L.; Maes, B.; Van Thourhout, D.; Baets, R. Tunable optical forces between nanophotonic waveguides. *Nat. Nanotechnol.* **2009**, *4*, 510–513.
- (24) Li, M.; Pernice, W. H.; Tang, H. X. Tunable bipolar optical interactions between guided lightwaves. *Nat. Photonics* **2009**, *3*, 464–468.
- (25) Rakich, P. T.; Popovic, M. A.; Soljacic, M.; Ippen, E. P. Trapping, corralling and spectral bonding of optical resonances through optically induced potentials. *Nat. Photonics* **2007**, *1*, 658–665.
- (26) Povinelli, M. L.; Lončar, M.; Ibanescu, M.; Smythe, E. J.; Johnson, S. G.; Capasso, F.; Joannopoulos, J. D. Evanescent-wave bonding between optical waveguides. *Opt. Lett.* **2005**, *30*, 3042–3044.
- (27) Zhao, R.; Tassin, P.; Koschny, T.; Soukoulis, C. M. Optical forces in nanowire pairs and metamaterials. *Opt. Express* **2010**, *18*, 25665–25676.
- (28) Falkovsky, L. A. Optical properties of graphene. *J. Phys.: Conf. Ser.* **2008**, *129*, 012004.
- (29) Gao, W.; Shu, J.; Qiu, C.; Xu, Q. Excitation of Plasmonic Waves in Graphene by Guided-Mode Resonances. *ACS Nano* **2012**, *6*, 7806–7813.
- (30) Stewart, J. *Calculus: Concepts and Contexts*; Brooks/Cole Cengage Learning: Belmont, CA, 2010.
- (31) Timoshenko, S.; Woinowsky-Krieger, S. *Theory of Plates and Shells*; McGraw-Hill, 1959.
- (32) Lu, Q.; Arroyo, M.; Huang, R. Elastic bending modulus of monolayer graphene. *J. Phys. D: Appl. Phys.* **2009**, *42*, 102002.
- (33) Sánchez-Portal, D.; Artacho, E.; Soler, J. M.; Rubio, A.; Ordejón, P. *Ab initio* structural, elastic, and vibrational properties of carbon nanotubes. *Phys. Rev. B: Condens. Matter Mater. Phys.* **1999**, *59*, 12678–12688.
- (34) Nicklow, R.; Wakabayashi, N.; Smith, H. G. Lattice Dynamics of Pyrolytic Graphite. *Phys. Rev. B* **1972**, *5*, 4951–4962.
- (35) Fasolino, A.; Los, J. H.; Katsnelson, M. I. Intrinsic ripples in graphene. *Nat. Mater.* **2007**, *6*, 858–861.
- (36) Atalaya, J.; Isacsson, A.; Kinaret, J. M. Continuum Elastic Modeling of Graphene Resonators. *Nano Lett.* **2008**, *8*, 4196–4200.
- (37) Lindahl, N.; Midtvedt, D.; Svensson, J.; Nerushev, O. A.; Lindvall, N.; Isacsson, A.; Campbell, E. E. B. Determination of the Bending Rigidity of Graphene via Electrostatic Actuation of Buckled Membranes. *Nano Lett.* **2012**, *12*, 3526–3531.
- (38) Snyman, J. *Practical Mathematical Optimization: An Introduction to Basic Optimization Theory and Classical and New Gradient-Based Algorithms*; Springer: New York, 2005.